MODELING FALSE ALARM RATE AND RELATED CHARACTERISTICS OF LIDAR AVALANCHE PHOTODIODE PHOTORECEIVERS

By Andrew S. Huntington, George M. Williams Jr., and Adam O. Lee
Allegro MicroSystems

ABSTRACT

An analysis is presented of the error introduced into estimates of avalanche photodiode (APD) lidar performance by assuming Gaussian distribution of the APD multiplication gain. The amplitude of current pulses emitted by an APD obeys the McIntyre distribution, the tails of which diverge from the Gaussian distribution having the same mean and variance. Because extinction of false alarms requires setting a discrimination threshold far into the tail of the output distribution of an analog photoreceiver, the threshold level required to achieve a specified false-alarm rate (FAR) using an APD-based photoreceiver is often not accurately predicted by the standard FAR model of Rice. [1] Characteristics of APD-based photoreceivers are calculated using the McIntyre distribution and are compared with characteristics calculated using the Gaussian approximation.

INTRODUCTION

Many lidar photoreceivers designed for the eye-safe spectral region near 1550 nm are assembled from InGaAs avalanche photodiodes (APDs) and resistive-feedback transimpedance amplifiers (RTIAs), followed by threshold pulse-detection and time-stamping circuits. This general photoreceiver configuration—whether deployed as a single-element sensor or as multiple parallel channels in a large-format sensor array—is applicable to lidar applications, such as autonomous vehicle navigation and hazard avoidance. InGaAs APDs are attractive for these applications because they are sensitive beyond a wavelength of 1.4 µm, where higher laser pulse energies can be used without creating an ocular hazard, and because the APD avalanche gain makes better use of weaker optical signals. Together, these qualities enable faster collection of three-dimensional scene data from longer range or using smaller-aperture optics. However, accurate modeling of electro-optic systems based on InGaAs APD photoreceivers requires an accurate model of the FAR of the APD photoreceiver, and the standard FAR model by Rice [1]—which is widely applied to photodiode-based photoreceivers—requires modification to accurately model false alarms from APD photoreceivers.

A simplified block diagram of the signal chain of a lidar APD photoreceiver is shown in Figure 1.

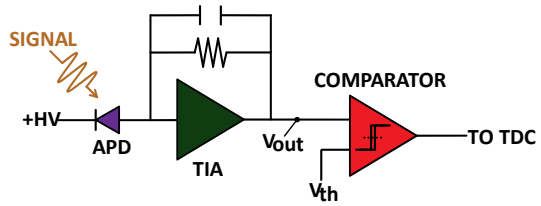

Figure 1: Block diagram of an APD-based lidar photoreceiver.

The APD converts incident optical power (watts) to an output photocurrent (amps); the transimpedance amplifier (TIA)—characterized by a conversion gain in ohms if its feedback is primarily resistive—then converts the photocurrent to a potential (volts). It is often convenient to work in units of quanta per signal pulse, such as photons for the optical signal and electrons for the output of the APD, in which case a conversion gain in units of reciprocal capacitance (e.g., V/e^-) can also be defined, based on the peak deflec-

[1] S. O. Rice, "Mathematical analysis of random noise," Bell Syst. Tech. J. 24(1), 46–156 (1945).

MCO-0001216
P0175

tion of the output voltage of the TIA in response to a current pulse containing a given electron count. In general, though, whether the conversion gain of the TIA is expressed in ohms or volts per electron, it is a function of photocurrent signal pulse shape because TIA bandwidth is finite and TIA gain spectra are not necessarily white. In the following discussion, a fixed photocurrent signal pulse shape that results in a fixed conversion gain is assumed.

The receiver diagrammed in Figure 1 is a leading-edge detector—one of the most common methods of time-of-flight lidar. The potential at the TIA output (V_{out}; see Figure 1) is fed into a threshold comparator that discriminates signal pulses from noise based on amplitude. When V_{out} passes through the detection threshold (V_{th}) with positive slope, a digital pulse is generated that is time-stamped by a time-to-digital converter.

If the comparator transitions upon reception of an optical signal, that event is a true positive; if the comparator transitions in the absence of a signal, that event is a false alarm. The pulse detection efficiency (P_d) of the photoreceiver is the ratio of true positives to transmitted pulses. Its FAR is the probability that, in the absence of a signal return, within an infinitesimal time interval (t, t + dt), the potential at the TIA output transitions through the detection threshold with positive slope.

A receiver operating characteristic (ROC) is a plot of the true-positive rate (TPR) compared with the false-positive rate (FPR) of a photoreceiver. If a lidar photoreceiver is operated using a range gate (t_{gate}) during which reception of a single pulse return is possible, then:

Equation 1:

$$TPR = P_d/t_{gate}\ (\text{Hz}).$$

Poisson statistics are used to calculate the FPR from the FAR, applying the definition that one or more false alarms during t_{gate} constitute a false positive. The probability of false positive (P_{FP}) is unity minus the probability of zero false alarms occurring during the range gate. The FPR is:

Equation 2:

$$FPR = \frac{P_{FP}}{t_{gate}} = \frac{1 - \exp(-FAR \times t_{gate})}{t_{gate}}\ (\text{Hz}).$$

Due to the term exp(–*FAR* × t_{gate}) in Equation 2, the ROC for a lidar photoreceiver depends on the range gate to which the probability of false positives applies. This prevents preparation of a general ROC for a lidar photoreceiver. However, a general plot of P_d against FAR can be computed that characterizes a receiver, which may informally be termed an ROC, as it permits easy computation of an ROC once the range gate has been specified. This latter type of ROC is analyzed in this paper.

The statistics of true positives and false alarms, which determine the ROC of a photoreceiver, depends on the pulse-height distributions of V_{out} when a signal is present (true positives) and when a signal is not present (false alarms). These distributions are illustrated graphically in Figure 2, where the solid curve is the distribution of V_{out} in the absence of a signal return, and the dashed curve is the distribution of V_{out} in the presence of a signal return. When a signal is received, the noise sources that cause V_{out} to vary under dark conditions—such as the amplifier circuit noise and the shot noise on dark current—are also present, such that the distribution of V_{out} when a signal is present is the convolution of its distribution under dark conditions with a separate distribution that characterizes the signal shot noise.

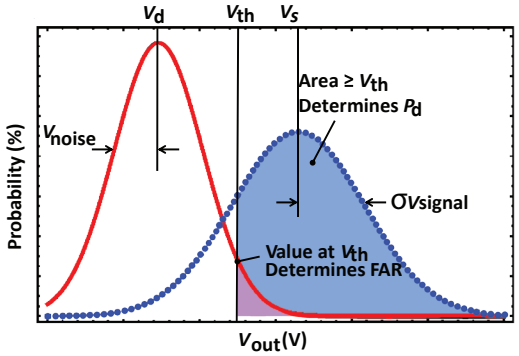

Figure 2: Statistical distributions of V_{out} for conditions with (dashed curves) and without (solid curves) the presence of an optical signal return.

The P_d is the fraction of an ensemble of identically prepared signal pulses that will result in $V_{out} \geq V_{th}$. Assuming that the photoreceiver is in an armed state where it is capable of responding to the reception of a signal pulse, P_d is the complementary cumulative distribution function (CCDF) of V_{out}, evaluated at V_{th}, in the presence of a signal return; graphically, the CCDF is the shaded area under the dashed curve in Figure 2.

Only part of the information required to compute the FAR is contained in Figure 2—the probability that, in the absence of signal, V_{out} passes through V_{th}. It is also necessary to determine the joint probability that V_{out} has positive slope as it passes through V_{th}. Rice [1] published equations for FAR based on the assumption that both V_{out} and its first time derivative are Gaussian distributed, using the bivariate

normal distribution in his foundational 1944/1945 paper "Mathematical analysis of random noise." To obtain accurate results for APD-based photoreceivers, Rice's equation must be modified to account for the amplitude distribution of the APD output, published by McIntyre [2] in 1972:

Equation 3:

$$P_{\mathrm{McIntyre}}(n) = \frac{p\,\Gamma\left(\frac{n}{1-k}+1\right)}{n(n-p)!\times\Gamma\left(\frac{nk}{1-k}+1+p\right)} \times\left[\frac{1+k(M-1)}{M}\right]^{p+\frac{nk}{1-k}} \times\left[\frac{(1-k)+(M-1)}{M}\right]^{n-p},$$

where p is the count of primary electrons injected into the APD multiplier, n is the count of output electrons resulting from p, k is the ionization rate ratio of the slower-ionizing carrier type to the faster-ionizing type (typically between 0.2 and 0.4 for InGaAs APDs), Γ is the Euler gamma function, and M is the mean avalanche gain at which the APD is operating.

The deviation of the McIntyre distribution from Gaussian—and its positive skew in particular—is more pronounced when a small number of primary electrons is multiplied (small p), when the mean avalanche gain is large (large M), and when the ionization rate ratio is closer to unity ($k \rightarrow 1$). This can be observed in the McIntyre distributions in Figure 3, which compares different values of p, M, and k with the same average output of $\langle n \rangle$ = 600 e$^-$. It is more important to use the McIntyre distribution to calculate FAR than P_d because the number of primary electrons in the zero-signal condition is much smaller than during signal reception and because the detection threshold of the photoreceiver must be set many standard deviations into the tail of the noise distribution to achieve technologically useful FAR, whereas differences in P_d smaller than a few percent are usually considered negligible. If the signal level is beyond the photon-counting regime (tens of photons or stronger), the Gaussian approximation is sufficiently accurate to calculate P_d.

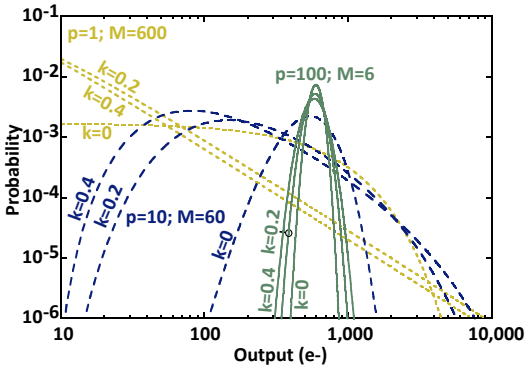

Figure 3: McIntyre distributions for different input electron counts (p), average gains (M), and ionization rate ratios (k) all resulting in an average output of 600 e⁻.

AVALANCHE PHOTODIODE PHOTORECEIVER OUTPUT STATISTICS

The output of an analog APD photoreceiver is the superposition of the output-voltage noise of the TIA with the voltage response of the TIA to the charge or current from the APD. The output of the APD is statistically independent from the noise of the TIA, so the random variable representing the output of the photoreceiver is the sum of two independent random variables, and its distribution is the convolution of their individual distributions.

The McIntyre distribution is a discrete electron-count distribution, so it is convenient to refer all quantities to the node between APD output and TIA input, and to work in units of electrons. Assuming a TIA conversion gain (G), then V_{out} and V_{th} are represented by equivalent charges at the TIA input ($n_{out} = V_{out}/G$ and $n_{th} = V_{th}/G$, respectively). Moreover, although V_{out} is a continuous variable that can take on any value as a result of circuit noise, the fluctuations of V_{out} due to the circuit noise of the TIA can be discretized and referred to the TIA input in units of charge. Writing the discrete probability distributions of the TIA input-referred noise and the APD output symbolically as P_{TIA} and P_{APD}, the probability that the output of the APD and the input-referred noise of the TIA will sum to a particular quantity of charge, n_{out}, is given by the discrete convolution:

Equation 4:

$$P_{RX}(n_{out}) = (P_{TIA} * P_{APD})(n_{out}) \equiv \sum_i P_{TIA}(i)\, P_{APD}(n_{out} - i).$$

[2] R. J. McIntyre, "The distribution of gains in uniformly multiplying avalanche photodiodes: theory," IEEE Trans. Electron Devices 19(6), 703–713 (1972)

This model presents some difficulties of interpretation because the noise of the TIA is an analog value characterized by the continuous Gaussian distribution of its output voltage, whereas the charge output of the APD is quantized and obeys the discrete McIntyre distribution. Furthermore, the McIntyre distribution does not address temporal statistics—it gives the probability that a certain number of electrons will eventually be output by an APD, yet it does not determine if all those output electrons will simultaneously contribute to the instantaneous current. Although the number of photons that arrive in a laser pulse and the number of photoelectrons generated by reception of that laser pulse are both discrete quantities, whether all of them contribute to n_{out} depends on the laser pulse shape and the frequency response of the TIA. A related issue is that, to apply the McIntyre distribution to FAR calculations, charge-integration times must be defined so that discrete electron counts can be computed from dark current and background photocurrent.

In practice, the lack of rigor inherent in using the Gaussian distribution as though it were a discrete distribution is not a serious difficulty for the noise levels and conversion gains that are characteristic of the TIAs used in lidar. As long as the voltage noise of the TIA is equivalent to hundreds of electrons or more at its input, little accuracy is lost if the random variable representing the input-referred noise of the TIA (n_{TIA}, in units of electrons) is restricted to integer values so that the Gaussian distribution function $P_{TIA}(n)$ can be interpreted as the probability of the TIA noise taking on a value within a band of a unit width centered on n_{TIA}. For the purpose of convolving $P_{TIA}(n_{TIA})$ with the output distribution of the APD:

Equation 5:

$$P_{\mathrm{TIA}}(n_{\mathrm{TIA}}) = \frac{1}{\sqrt{2\pi \mathrm{var}(n_{\mathrm{TIA}})}} \exp\left[-\frac{(n_{\mathrm{TIA}} - \bar{n}_{\mathrm{TIA}})^2}{2\mathrm{var}(n_{\mathrm{TIA}})}\right],$$

where $\bar{n}_{TIA}$ is the mean output-voltage level of the TIA in the absence of a signal divided by G, and var(n_{TIA}) is the square of the output noise referred to the TIA input in units of electrons. It should be noted that although the TIA is characterized by a fixed output-voltage noise, the conversion gain depends on signal pulse shape, so the input-referred noise of the TIA depends on the pulse shape of the signal to which it is referenced.

Primary (unmultiplied) dark current and photocurrent are generated by Poisson processes, so the APD output distribution in the convolution of Equation 4 must account for the distribution of the primary electron count (p) in Equation 3. A Poisson-weighted sum of McIntyre distributions is used:

Equation 6:

$$P_{\mathrm{APD}}(n) = \sum_{p} P_{\mathrm{Poisson}}(p) \times P_{\mathrm{McIntyre}}(n)$$

$$= \sum_{p} \exp\left(-\langle p \rangle\right) \frac{\langle p \rangle^{p}}{p!} \times P_{\mathrm{McIntyre}}(n).$$

In the dark condition, the primary direct-current (DC) dark current and background photocurrent integrate to an average electron count $\langle p_{DC} \rangle$. Reception of an optical pulse generates p_{signal} primary carriers and, because the DC current is also present, the average primary electron count in the illuminated condition is:

Equation 7:

$$\langle p \rangle = \langle p_{\mathrm{DC}} \rangle + \langle p_{signal} \rangle.$$

In Figure 2, assuming the TIA contributes no offset, the mean voltage when no signal is present (V_{dark}) is expressed as:

Equation 8:

$$V_{\mathrm{dark}} = G \times M \times \langle p_{DC} \rangle \ (\mathrm{V}),$$

and the mean output voltage when a signal is present (V_{signal}) is expressed as:

Equation 9:

$$V_{\mathrm{signal}} = G \times M \times (\langle p_{DC} \rangle + \langle p_{signal} \rangle) \ (\mathrm{V}).$$

To clarify the effective integration times that relate APD currents to the primary electron counts p_{DC} and p_{signal}—as well as to the multiplied output electron count in Equation 3—it is helpful to consider two limiting amplifier cases: 1) an ideal RTIA that generates an instantaneous output voltage proportional to the instantaneous output current of the APD; and 2) a switched capacitive-feedback transimpedance amplifier (CTIA), similar to those used in many imaging readout integrated circuits, where an output voltage is generated that is proportional to the total charge delivered by the APD during some fixed exposure time.

In the case of an ideal RTIA, the response of the photoreceiver is not determined by the total number of electrons generated from the photons received in a signal pulse, but rather by the maximum photocurrent that flows as a result. The Shockley–Ramo theorem allows the instantaneous current at the terminals of an APD, $i(t)$, to be calculated from the instantaneous count of electrons and holes within its junc-

tion, $n_e(t)$ and $n_h(t)$, and their respective saturation velocities in units of cm/s, v_{se} and v_{sh}, as [3],[4],[5]:

Equation 10:

$$i(t) \approx \frac{q}{w}\,[v_{se}n_e(t) + v_{sh}n_h(t)]\ (\mathrm{A}),$$

where q is the elementary charge in Coulombs, and w is the junction width in cm.

Equation 10 can be recast in terms of junction transit times for electrons ($t_e = w/v_{se}$) and holes ($t_h = w/v_{sh}$) as:

Equation 11:

$$i(t) \approx q\left[\frac{n_e(t)}{t_e} + \frac{n_h(t)}{t_h}\right]\ (\mathrm{A}).$$

If the laser pulse is much shorter than both junction transit times, then all of the carriers generated from the pulse will be present inside the junction simultaneously, and the APD output pulse-height distribution can be calculated using the average photon number of the laser pulse (N_{signal}) and the primary quantum efficiency (QE) of the APD to find the mean primary photoelectron count:

Equation 12:

$$\langle p_{signal}\rangle = QE \times N_{signal},$$

and the mean multiplied signal electron count:

Equation 13:

$$\langle N_{signal}\rangle = \langle p_{signal}\rangle \times M.$$

If, however, the laser pulse duration (t_{pulse}) is longer than the junction transit time, only a portion of the pulse energy will contribute to the response of the ideal RTIA photoreceiver. For a rectangular pulse of duration t_{pulse} in seconds, the average primary electron count resulting from a signal pulse is approximately:

Equation 14:

$$\langle p_{signal}\rangle \approx QE \times N_{signal}\,[t_e/t_{pulse}].$$

A calculation similar to Equation 14 applies to the combined dark current (I_{dark}) and background photocurrent ($I_{background}$), regardless of whether the signal pulse is longer or shorter than the junction transit time. I_{dark} and $I_{background}$ are both generated by Poisson processes and, for most SWIR APD designs, the majority of the dark current originates in the InGaAs light-absorption layer because, of the materials from which the device is fabricated, the InGaAs alloy has the narrowest bandgap. Consequently, dark current and background photocurrent experience the same avalanche gain statistics and can be grouped into a single quantity, I_{DC}. The associated average primary electron count from this combined DC current is then:

Equation 15:

$$\langle p_{DC}\rangle \approx \frac{I_{dark} + I_{background}}{qM}t_e = \frac{I_{DC}}{qM}t_e,$$

where I_{dark} and $I_{background}$ are both in units of amps.

The average multiplied electron count from dark current and background photocurrent is:

Equation 16:

$$\langle n_{DC}\rangle = \langle p_{DC}\rangle \times M.$$

When the TIA does not have a separate output-voltage offset, $\langle n_{DC}\rangle$ is the input-referred form of V_{dark}, and Equation 16 is a restatement of Equation 8.

In the case of a switched CTIA, charge from the APD may be accumulated over a current integration time (t_{int}) that is longer than t_e. In that case, t_{int} replaces t_e in Equation 14 and Equation 15. However—because dark current from the detector integrates too quickly, a ramped detection threshold that exactly tracks the charge integrated since the last reset is difficult to implement, and the settling time following a switched reset is too long—it is impractical to use switched CTIAs for lidar. Instead, CTIAs that are continuously reset through a low-pass filter or RTIAs that have some integrating characteristics are commonly employed. The simplest example of the latter is an RTIA with insufficient bandwidth to match the rise time of the photocurrent pulse from the APD. When the bandwidth of an RTIA is too low for V_{out} to track the input photocurrent waveform, the photocurrent charge deposited on its input shifts the input potential from virtual ground. Current flows in the feedback resistor of the RTIA until the potential at the input has been restored to its normal operating point, effectively giving the RTIA

[3] W. Shockley, "Currents to conductors induced by a moving point charge," J. Appl. Phys. 9(10), 635–636 (1938).

[4] S. Ramo, "Currents induced by electron motion," Proc. IRE 27(9), 584– 585 (1939).

[5] M. M. Hayat et al., "Gain-bandwidth characteristics of thin avalanche photodiodes," IEEE Trans. Electron Devices 49(5), 770–781 (2002).

some charge-integrating characteristic. This is not helpful in a telecommunications application, where rapid settling is required to resolve "0" symbols following "1" symbols. The canonical "eye diagram" closes when the receiver circuit cannot keep pace with the optical modulation. However, lidar is different because the optical pulses are very sparse—typically once per 100 ms, and no faster than once per 1 µs—so rise times in the order of tens of nanoseconds do not hamper reception of consecutive pulses.

For either the case of a continuously reset CTIA or a real-world RTIA, an effective DC current integration period (t_{DC}) can be extracted from circuit simulations for use in place of t_e in Equation 15. The same circuit simulation produces a pulse-shape-specific value of the conversion gain; this value is used instead of Equation 14 to determine the signal response. Unfortunately, because the details of the transfer function of the TIA determine the quantitative relationship between the voltage noise at the TIA output and fluctuations of I_{dark} and $I_{background}$ at the TIA input, it is usually not possible to apply analytic methods to estimate t_{DC} with useful accuracy. Instead, a *simulation program with integrated circuit emphasis* (SPICE) model of the TIA can be used to arrive at t_{DC}. In such a SPICE model, the APD is represented by a DC current source equal to I_{DC}, a transient-current source waveform of $I_{AC}(t)$ as derived from the laser pulse shape, a capacitor corresponding to the junction and interconnect capacitance of the APD, and a current noise source of spectral intensity (S_I). InGaAs APDs typically operate with subnanosecond rise time so, for most nanosecond-scale pulses used in lidar, the transient part of the current source can be approximated as the product of the APD spectral responsivity (R) and the optical-power waveform of the signal pulse, $P(t)$:

Equation 17:

$$I_{AC}(t) = R \times P(t)\ (\mathrm{A}),$$

where $P(t)$ is in units of watts, and the spectral responsivity of the APD is:

Equation 18:

$$R = M \times QE(\lambda/1.23984)\ (\mathrm{A/W}),$$

where λ is the laser wavelength in micrometers.

The spectral intensity of the current noise source that models multiplied shot noise on the dark current and background photocurrent is:

Equation 19:

$$S_{I_{DC}} = 2qMFI_{DC}\ (\mathrm{A^2/Hz}),$$

where the excess noise factor (F) is [2]:

Equation 20:

$$F = M\left[1 - (1-k)\left(\frac{M-1}{M}\right)^2\right].$$

SPICE models cannot simulate the full amplitude distribution of noise modeled by Equation 4. However, the standard noise deviation of V_{out} is accessible. The procedure for extracting t_{DC} from a SPICE model of an APD photoreceiver is to simulate the RMS noise on V_{out}, in the absence of an optical signal, both with the noise source representing the APD (V_{noise}) and without the noise source representing the APD (V_{noise} TIA). The noise contributed by the TIA is uncorrelated with the noise contributed by the APD, so the voltage noise attributable to the combined dark current and background photocurrent is:

Equation 21:

$$V_{\mathrm{noiseAPD}} = \sqrt{V_{\mathrm{noise}}^2 - V_{\mathrm{noiseTIA}}^2}\ \ (\mathrm{V\ RMS}).$$

Conversion gain for the specific pulse shape modeled by $I_{AC}(t)$ is extracted from the SPICE simulation by dividing the swing in V_{out} in response to $I_{AC}(t)$ by the total integrated charge delivered by $I_{AC}(t)$:

Equation 22:

$$G = \frac{V_{\mathrm{signal}} - V_{\mathrm{dark}}}{\frac{1}{q}\int I_{\mathrm{AC}}(t)\mathrm{d}t}\ (\mathrm{V/e^-}),$$

where V_{signal} and V_{dark} are the peak output voltage response from the SPICE simulation and the output voltage in the absence of a signal, respectively. It is important to note that Equation 17 defines $I_{AC}(t)$ at the output of the APD, and any coupling loss resulting from impedance mismatch between the APD and the TIA must be factored into the SPICE model.

The conversion gain is used to express the RMS voltage noise associated with the APD dark current and background photocurrent in units of electrons:

Equation 23:

$$n_{\mathrm{noiseAPD}} = \frac{V_{\mathrm{noiseAPD}}}{G}(\mathrm{e^-}).$$

The same relationship defines the TIA input-referred charge noise ($n_{noiseTIA}$), the square of which is equal to the variance appearing in Equation 5:

Equation 24:

$$\mathrm{var}(n_{TIA}) = n^2_{noiseTIA} = \left(\frac{V_{noiseTIA}}{G}\right)^2 \ (e^{-2}).$$

The noise-equivalent input (NEI) of the photoreceiver is found using G to refer the output-voltage noise in the zero-signal condition (V_{noise}) to an equivalent amount of input charge (n_{noise}) and using the product of the mean gain and QE of the APD to refer V_{noise} to an equivalent input level in photons:

Equation 25:

$$\mathrm{NEI} = \frac{V_{noise}}{G \times QE \times M} \ (\mathrm{photons}).$$

The effective DC current integration time for use in Equation 15 is found by equating the value for $n_{noiseAPD}$ given by the SPICE model to the value given by the Burgess variance theorem, [6],[7] which underlies the noise-current spectral-intensity theorem of Equation 19:

Equation 26:

$$n^2_{noiseAPD} = \langle p_{DC} \rangle M^2 F = \left(\frac{I_{DC}}{qM} t_{DC}\right) M^2 F$$
$$\Rightarrow t_{DC} = \frac{q n^2_{noiseAPD}}{I_{DC} M F} \ (\mathrm{s}).$$

This calculation arrives at a value for t_{DC} that is calibrated such that an analytic calculation of the variance of V_{out} matches a SPICE simulation, properly accounting for the transfer function of the TIA acting on the APD noise spectrum, which Equation 19 models as white within the TIA bandwidth. With t_{DC}, the full noise distribution of the APD photoreceiver can be computed using Equation 4. It should be emphasized that, because the conversion gain is used to relate output-voltage levels to input electron count, the input-referred charge noise as well as t_{DC} is the function of the laser pulse shape. Conversion gain for pulses with a greater fraction of their energy outside the gain spectrum of the TIA will be lower, resulting in larger values of input-referred charge noise such as $n_{noiseAPD}$ and, therefore, larger values of t_{DC}.

These methods were applied to compute $P_{RX}(n_{out})$ for a lidar photoreceiver assembled from a 75 µm-diameter InGaAs APD characterized by 80% QE at 1550 nm, k = 0.2, and I_{dark} = 2.2 nA when operating at M = 10. The APD was paired with a TIA characterized by a 3 dB bandwidth of 31 MHz, and—when responding to 4 ns full width at half maximum Gaussian-shaped laser pulses—t_{DC} = 10.2 ns and $n_{noiseTIA}$ = 244 e⁻. With these parameters, $\langle p_{DC} \rangle$ = 14 e⁻ at M = 10. The photoreceiver output distribution was calculated for dark conditions (no signal or background photocurrent), with the APD operating at mean avalanche gains of M = 5, 10, and 20. The distributions computed by the convolution of Equation 4 are compared in Figure 4 to Gaussian distributions having the same means and variances. In this case, at avalanche gains greater than about M = 10, the divergence of the high-output tails of the photoreceiver distributions from their Gaussian approximations causes an FAR model based on the Gaussian approximation to underpredict the value of V_{th} required to extinguish false alarms below a given rate.

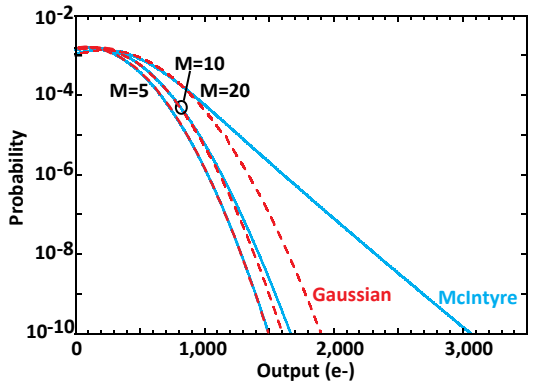

Figure 4: Comparison of APD photoreceiver output distributions (solid curves) to Gaussian approximations having the same means and variances (dashed curves).

P_d AND FAR FOR APD PHOTORECEIVERS

The probability of detecting a signal return pulse is the conditional probability that: 1) the photoreceiver is ready to register the pulse at the time it arrives; and 2) the pulse into the decision circuit exceeds the detection threshold. Because the decision circuit only fires when its input voltage rises through its detection threshold, assuming that the laser pulse repetition period is many multiples of the settling time (t_{settle}) of the amplifier, the probability that the receiver is active at the time a signal pulse arrives is the probability that zero false alarms have occurred within the preceding t_{settle}. We can estimate $t_{settle} \approx 2t_{rise} \approx 0.7/BW$ and compute:

[6] R. E. Burgess, "Homophase and heterophase fluctuations in semicon- ductor crystals," Discuss. Faraday Soc. 28, 151–158 (1959).

[7] R. E. Burgess, "Some topics in the fluctuation of photo-processes in solids," J. Phys. Chem. Solids 22, 371–377 (1961).

Equation 27:

$$P_d \approx \exp\left(-\frac{0.7}{\mathrm{BW}}\mathrm{FAR}\right) \times \left[1 - \sum_{n_{\mathrm{out}} \le n_{\mathrm{th}}} P_{\mathrm{RX}}(n_{\mathrm{out}})\right],$$

where t_{rise} is the 10%-to-90% rise time in seconds and BW is the 3 dB bandwidth in Hertz.

Assuming typical design and operation—with FAR < 1 kHz and BW > 10 MHz—the exponential prefactor is essentially unity, and the detection efficiency is given by the second quantity—the CCDF of P_{RX} evaluated at the detection threshold. The exponential prefactor is primarily relevant in the photon-counting regime, when receivers may operate with detection threshold closer to the noise floor to sense weak signals, resulting in high FAR. When the average signal level is in the order of 10 photons or fewer, the divergence of the McIntyre distribution from its Gaussian approximation is large enough (Figure 3) that it may be advisable to compute P_d using Equation 27. However, outside the photon-counting regime, the Gaussian approximation may be used, resulting in:

Equation 28:

$$P_d \approx \frac{1}{2}\left\{1 - \mathrm{erf}\left[\frac{n_{\mathrm{th}} - (\langle n_{\mathrm{DC}}\rangle + \langle n_{\mathrm{signal}}\rangle)}{\sqrt{2(n^2_{\mathrm{noiseTIA}} + (\langle n_{\mathrm{DC}}\rangle + \langle n_{\mathrm{signal}}\rangle))MF}}\right]\right\},$$

where, assuming no offset due to the TIA, $\langle n_{DC}\rangle$ is found from Equation 15 and Equation 16, using t_{DC} and $\langle N_{signal}\rangle = N_{signal} \times QE \times M$. Note that, if the detection threshold ($n_{th} = V_{th}/G$) is referenced to the mean output voltage in the dark condition (V_{dark}), then the mean DC offset ($\langle n_{DC}\rangle = V_{dark}/G$) can be omitted from the numerator inside the error function in Equation 28.

In the case of an RTIA characterized by transimpedance (G_Ω in ohms) and BW in Hz, responding to a laser pulse of peak power P_{signal} in watts, P_d can also be written as:

Equation 29:

$$P_d \approx \frac{1}{2}\left[1 - \mathrm{erf}\left(\frac{V_{\mathrm{th}} - [R(P_{\mathrm{signal}} + P_{\mathrm{background}}) + I_{\mathrm{dark}}]G_\Omega}{G_\Omega\sqrt{2\{2qMF[R(P_{\mathrm{signal}} + P_{\mathrm{background}}) + I_{\mathrm{dark}}] + S_{I\_\mathrm{TIA}}\}\mathrm{BW}}}\right)\right],$$

where it is assumed that a narrow bandpass optical filter restricts the spectrum of the background illumination to the laser wavelength, $P_{background}$ is the transmitted background optical power in units of watts, and the input-referred noise-current spectral intensity of the TIA (S_{I_TIA}) is in units of A^2/Hz. One merit of Equation 29 is that G_Ω, BW, and S_{I_TIA} are specified by most RTIA manufacturers, permitting calculations without SPICE simulation. However, the same transimpedance value (G_Ω) in Equation 29 is assumed to apply equally to the peak of the signal photocurrent pulse and to the APD current shot noise. The case in which the RTIA bandwidth is too low for V_{out} to track the input photocurrent waveform—which is the configuration that often maximizes receiver sensitivity, given operational constraints on FAR and timing precision—is not modeled by Equation 29.

In developing an expression for FAR that accounts for the non-Gaussian distribution of APD output, we follow the Rice [1] calculation of the Gaussian case. Rice analyzes a noisy current waveform defined in terms of uncorrelated random variables for its current (I) and the slope of its current (η) at every point in time, t. A false alarm occurs when the current transitions through a threshold value (I_{th}) with a positive slope. Rice shows that the probability of this occurring during the infinitesimal time interval (t, $t + dt$) is:

Equation 30:

$$\mathrm{PDF}_{\mathrm{FA}} = \mathrm{d}t\int_0^\infty \eta P(I = I_{\mathrm{th}}, \eta; t)\mathrm{d}\eta \ (\mathrm{Hz}),$$

where $P(I = I_{th},\eta;t)$ is the joint probability distribution of the current and its slope at time t, assuming the random variable for the current has the value I_{th}. The classic result of Rice for FAR applies to Gaussian-distributed noise, for which $P(I = I_{th},\eta;t)$ is the bivariate normal distribution. In the case of two uncorrelated random variables, the bivariate normal distribution is the product of two single-variable Gaussian distributions:

Equation 31:

$$P(I, \eta; t)\mathrm{Gaussian} = \frac{1}{2\pi\sqrt{\mathrm{var}(I)\mathrm{var}(\eta)}} \times \exp\left[\frac{1}{2}\left(\frac{[I - \bar{I}]^2}{\mathrm{var}(I)} + \left(\frac{[\eta - \bar{\eta}]^2}{\mathrm{var}(\eta)}\right)\right]\right] (\mathrm{A^{-2}Hz^{-1}}).$$

Noting that—for $I(t)$ not to diverge—the average slope ($\bar{\eta}$) has to be zero, and substitution of Equation 31 in Equation 30 gives:

Equation 32:

$$\mathrm{PDF}_{\mathrm{FA\_Gaussian}} = \frac{\mathrm{d}t}{2\pi}\sqrt{\frac{\mathrm{var}(\eta)}{\mathrm{var}(I)}}\exp\left[-\frac{1}{2}\left(\frac{[I_{\mathrm{th}} - \bar{I}]^2}{\mathrm{var}(I)}\right)\right] (\mathrm{Hz}).$$

The FAR is Equation 32 without the differential dt.

Rice relates the variances of the current and its slope to its autocorrelation function (ψ) at zero time lag (τ) as (respectively):

Equation 33:

$$\mathrm{var}(I) = \Psi_0 \equiv \lim_{t\to\infty} \frac{1}{t}\int_0^t I(t)I(t+\tau)\mathrm{d}t\Big|_{\tau=0} \ (\mathrm{A}^2); \text{ and}$$

Equation 34:

$$\mathrm{var}(\eta) = -\Psi_0'' \equiv -\frac{\partial^2}{\partial\tau^2}\Psi\Big|_{\tau=0} \ (\mathrm{A}^2/\mathrm{s}^2).$$

The autocorrelation function is itself related to the spectral intensity of the noisy current by inversion of the Wiener–Khintchine theorem [8],[9],[10]:

Equation 35:

$$\Psi(\tau) = \int_0^\infty S_I(f)\cos(2\pi f\tau)\mathrm{d}f \ (\mathrm{A}^2).$$

Therefore:

Equation 36:

$$\mathrm{var}(I) = \Psi_0 = \int_0^\infty S_I(f)\mathrm{d}f \ (\mathrm{A}^2);$$

Equation 37:

$$\mathrm{var}(\eta) = 4\pi^2\int_0^\infty f^2 S_I(f)\mathrm{d}f \ (\mathrm{A}^2/\mathrm{s}^2).$$

Substituting Equation 36 and Equation 37 into Equation 32, the FAR for Gaussian-distributed noise is:

Equation 38:

$$\mathrm{FAR}_{\mathrm{Gaussian}} = \frac{1}{2\pi}\sqrt{\frac{4\pi^2\int_0^\infty f^2 S_I(f)\mathrm{d}f}{\int_0^\infty S_I(f)\mathrm{d}f}} \times \exp\left\{-\frac{1}{2}\left[\frac{(I_{\mathrm{th}}-\bar{I})^2}{\mathrm{var}(I)}\right]\right\}(\mathrm{Hz}),$$

where $\mathrm{var}(I) = V_{\mathrm{noise}}^2/G_\Omega^2$ is the variance of the current in the dark condition, $I_{\mathrm{th}} = V_{\mathrm{th}}/G_\Omega$ is the detection threshold expressed as an equivalent current at the TIA input, and $\bar{I} = V_{\mathrm{dark}}/G_\Omega$ is the average DC current level in the dark condition. In the absence of a voltage offset associated with the TIA, $\bar{I} = I_{\mathrm{DC}}$, and if the threshold voltage is referenced to V_{dark}, $\bar{I} = 0$.

When the noise spectrum is white (constant S_I) over a finite bandwidth, S_I cancels out in the radical and Equation 38 becomes:

Equation 39:

$$\mathrm{FAR}_{\mathrm{Gaussian}} = \sqrt{\frac{1}{3}}\mathrm{BW}\ \exp\left[-\frac{(I_{\mathrm{th}}-\bar{I})^2}{2I_{\mathrm{noise}}^2}\right] = \sqrt{\frac{1}{3}}\mathrm{BW}\ \exp\left[-\frac{(V_{\mathrm{th}}-V_{\mathrm{dark}})^2}{2V_{\mathrm{noise}}^2}\right](\mathrm{Hz}),$$

where the TIA transimpedance relates the input-referred current quantities I_{th}, $\bar{I}$, and I_{noise} to the corresponding output-voltage quantities V_{th}, V_{dark}, and V_{noise} diagramed in Figure 2. The variance of the current in the dark condition, var(I), is found from the noise spectral intensity of the dark current and background photocurrent, S_{I_DC}, given by Equation 19, and the input-referred noise-current spectral intensity of the TIA (S_{I_TIA}):

Equation 40:

$$I_{\mathrm{noise}}^2 = \mathrm{var}(I) = \mathrm{BW}\times(S_{I\_\mathrm{TIA}} + S_{I\_\mathrm{DC}}) = \mathrm{BW}\times[S_{I\_\mathrm{TIA}} + 2qMF(I_{\mathrm{DC}})]\ (\mathrm{A}^2).$$

Within the Gaussian approximation, the threshold that must be set to achieve a specified FAR is found from Equation 39 as:

Equation 41:

$$\frac{V_{\mathrm{th}}-V_{\mathrm{dark}}}{V_{\mathrm{noise}}} = \frac{I_{\mathrm{th}}-\bar{I}}{I_{\mathrm{noise}}} = \sqrt{-2\ln\left(\frac{\sqrt{3}\mathrm{FAR}}{\mathrm{BW}}\right)}.$$

Calculating FAR with better accuracy at threshold levels set high in the tail of the output distribution of an APD photoreceiver requires using the convolution of the McIntyre-distributed output of the APD with the Gaussian-distributed TIA

[8] N. Wiener, "Generalized harmonic analysis," Acta Math. 55, 117–258 (1930).

[9] A. Khintchine, "Korrelationstheorie der stationären stochastischen Prozesse," Math. Ann. 109(1), 604–615 (1934).

[10] A. Van Der Ziel, Noise in Solid State Devices and Circuits, pp. 10–12, John Wiley and Sons, New York (1986).

noise, $P_{RX}(n_{out})$, given by Equation 4, in place of the Gaussian distribution used by Rice. $P_{RX}(n_{out})$ is an electron-count distribution (referred to the node between the APD and the TIA), but it can be used for the current distribution through a change of variable. Assuming the charge associated with electron count (n_{out}) is transported in time (t_{ref}), the current can be rewritten:

Equation 42:

$$I = \frac{q}{t_{ref}}\, n_{out}\,(\mathrm{A}^2).$$

Following the rule for change of variable of a probability density function, the current distribution is:

Equation 43:

$$P_{RX}(I) = \left|\frac{d}{dI}\, n_{out}(I)\right| P_{RX}\,[n_{out}(I)] = \frac{t_{ref}}{q}\; P_{RX}(n_{out})\;\; (\mathrm{A}^{-1}).$$

The joint probability distribution of the current and its slope, equivalent to Equation 31, is:

Equation 44:

$$P(I, \eta; t)_{McIntyre} = \frac{1}{\sqrt{2\pi \mathrm{var}(\eta)}}\; \frac{t_{ref}}{q}\, P_{RX}(n_{out}) \times \exp\left[-\frac{\eta^2}{2\mathrm{var}(\eta)}\right]\; (\mathrm{A}^{-2}\mathrm{Hz}^{-1}).$$

Substitution of the modified joint probability distribution into Equation 30 gives:

Equation 45:

$$\mathrm{PDF}_{FA\_McIntyre} = \frac{dt}{2\pi}\; \sqrt{\frac{\mathrm{var}(\eta)}{\mathrm{var}(I)}}\; \frac{t_{ref}}{q}\, P_{RX}(n_{th})\, \sqrt{2\pi \mathrm{var}(I)}\;\; (\mathrm{Hz});\ \text{and}$$

Equation 46:

$$\mathrm{FAR}_{McIntyre} = \sqrt{\frac{2\pi}{3}}\;\; \frac{t_{ref}}{q} I_{noise}\, \mathrm{BW} P_{RX}(n_{th})\;(\mathrm{Hz}).$$

To use Equation 46, t_{ref} must be explicitly defined. Rice's equation for FAR based on Gaussian-distributed noise, Equation 39, is recovered from Equation 46 if the substitution $n_{th} = (t_{ref}/q)I_{th}$ is made to express the threshold voltage in terms of an equivalent input current rather than an equivalent input electron count, and a discretized Gaussian distribution of mean $\langle n_{DC}\rangle = (t_{ref}/q)I_{DC}$ and variance $n^2_{noise} = \mathrm{var}(n_{out}) = [(t_{ref}/q)I_{noise}]^2$ is used in place of the convolution for $P_{RX}(n_{th})$. The Burgess variance theorem is used to calculate the APD contribution to n^2_{noise}, resulting in:

Equation 47:

$$n^2_{noise} = n^2_{noiseTIA} + n^2_{noiseAPD} = n^2_{noiseTIA} + \frac{t_{ref}}{q}\, I_{DC} MF\;(\mathrm{e}^{-2}).$$

From Equation 47, it is found that the relationship $n^2_{noise} = [(t_{ref}/q)I_{noise}]^2$ is equivalent to setting t_{ref} equal to $1/(2BW)$. In other words, within the approximations of a white noise spectrum and a flat TIA frequency response, the effective DC current integration time is $1/(2BW)$. Alternatively, if t_{DC} and $n_{noiseTIA}$ have been obtained from SPICE simulations, the FAR of Equation 46 can be expressed as:

Equation 48:

$$\mathrm{FAR}_{McIntyre} = \sqrt{\frac{2\pi}{3}}\, n_{noise} \mathrm{BW} P_{RX}(n_{th})\;(\mathrm{Hz}).$$

It is important that n_{th} be consistently defined if Equation 48 is used to find a threshold corresponding to a specified FAR and that Equation 28 then be used to determine the signal-detection probability at that threshold. As noted earlier, if V_{th} is measured in the lab relative to V_{dark}, the DC offset $\langle n_{DC}\rangle$ is omitted from the numerator of Equation 28 for P_d. This treatment is consistent with omitting V_{dark} or $\bar{I}$ from the $(V_{th} - V_{dark})$ or $(I_{th} - \bar{I})$ expressions in the Gaussian FAR models of Equation 39 and Equation 41. However, when the convolution $P_{RX}(n_{out})$ defined in Equation 4 is used with Equation 48 for FAR, the value of n_{out} that maps to a given FAR is not referenced to $\langle n_{DC}\rangle$. Consequently, the offset $\langle n_{DC}\rangle$ must be retained in the numerator of Equation 28 for P_d calculations based on threshold levels found from Equation 4 and Equation 48.

In Figure 5, FARs calculated by the Gaussian approximation of Equation 39 are compared with those calculated using Equation 48, based on the same photoreceiver parameters as Figure 4. FARs in the vicinity of 10 to 100 Hz are of technological interest, and it can be observed from Figure 5 that, in this case, the Gaussian approximation underestimates the detection threshold required to operate with a FAR below 10 Hz at an APD gain of $M = 20$ by about 34%. The size of the discrepancy is strongly dependent on APD gain as well as the relative magnitude of APD shot noise compared with TIA circuit noise. In the case graphed in Figure 5, amplifier noise dominates, with $n_{noiseTIA} = 244\ \mathrm{e}^-$; at $M = 10$, $n_{noiseAPD} = 71\ \mathrm{e}^-$; and at $M = 20$, $n_{noiseAPD} = 160\ \mathrm{e}^-$. When the APD noise is more dominant, such as for photoreceivers

assembled from larger-diameter APDs or those characterized by larger values of *k*—or when any APD photoreceiver is operated at higher avalanche gain—the skew of the McIntyre distribution has a larger impact on the FAR versus threshold characteristic.

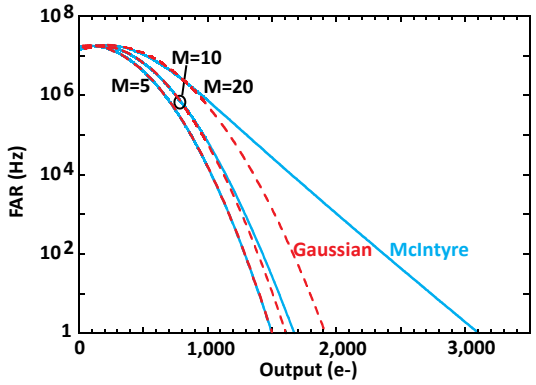

Figure 5: Comparison of FAR versus detection threshold characteristics computed using either the convolution model of P_{RX} (solid curves) or its Gaussian approximation (dashed curves).

PHOTORECEIVER PERFORMANCE AND RECEIVER OPERATING CHARACTERISTIC

The signal level required to achieve 99% P_d is shown in Figure 6 as a function of FAR, for different APD gains. The photoreceiver parameters are the same as those used in Figure 4 and Figure 5. Sensitivity improves as the gain increases from $M = 10$ to $M = 20$. The plot also shows that the optimal APD gain is closer to $M = 15$ than $M = 20$ because, at $M > 10$, the threshold required to extinguish false alarms diverges from the Gaussian model, as shown in Figure 5. This fact is missed by the sensitivity calculation based on the Gaussian approximation, which predicts lower overall signal levels and shows $M = 20$ to be superior to $M = 15$.

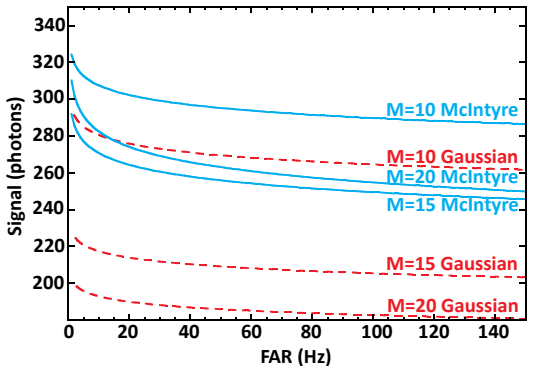

Figure 6: Mean signal level required to achieve $P_d = 99\%$ as calculated at different APD gains using either the convolution model of P_{RX} (solid curves) or its Gaussian approximation (dashed curves).

A plot of P_d versus FAR at a mean signal level of 250 photons for the same receiver is presented in Figure 7. An ROC for a specified range gate can be computed from this information using Equation 2.

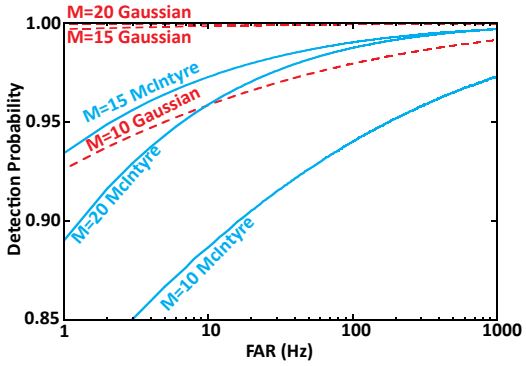

Figure 7: P_d versus FAR at three different APD gains, for a mean signal level of 250 photons, calculated using either the convolution model of P_{RX} (solid curves) or its Gaussian approximation (dashed curves).

The NEI and sensitivities for FAR = 150 Hz at 95% and 99% P_d are plotted in Figure 8 as functions of avalanche gain, at different operating temperatures. The NEI, which is calculated from the standard deviation of V_{out}, is, compared with FAR, less sensitive to the tail of the distribution. This is evident in Figure 8, where, at 27°C and 50°C, the gain that minimizes NEI is less than the gain that achieves the best sensitivity at the specified FAR. The optimal gain at −40°C is greater than at the other temperatures, owing to less APD dark current because it is the APD that generates the higher-amplitude false alarms that necessitate setting higher detection thresholds than predicted by the Gaussian noise model.

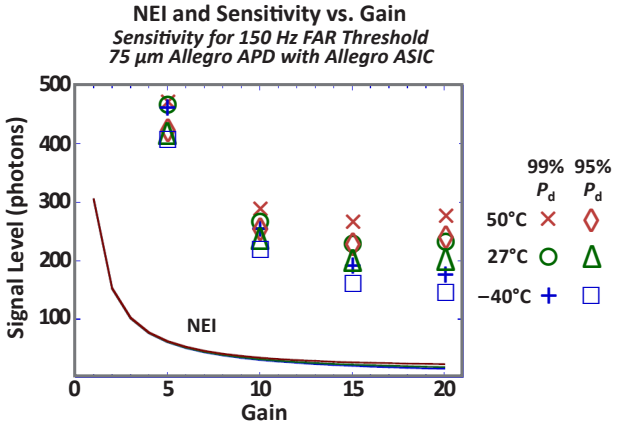

Figure 8: NEI and sensitivity for FAR = 150 Hz at $P_d = 95\%$ and 99% versus avalanche gain at −40°C, 27°C, and 50°C, modeled from empirical 75 µm Allegro photoreceiver dark current, excess noise, and NEI data.

The ratios between 95% and 99% sensitivity and NEI are plotted in Figure 9. This ratio is related to the ratio between threshold and noise given by Equation 41,

being close to $[(n_{th} - \langle n_{DC} \rangle)/n_{noise}] + 1.65$ for $P_d = 95\%$ and $[(n_{th} - \langle n_{DC} \rangle)/n_{noise}] + 2.4$ for $P_d = 99\%$; for $P_d = 50\%$, Equation 41 is the same as the sensitivity-to-NEI ratio. Equation 41 gives $[(n_{th} - \langle n_{DC} \rangle)/n_{noise}] \approx 4.85$ for BW = 31 MHz and FAR = 150, and as M→1, the 95% and 99% sensitivity-to-NEI ratio converge on the values of 6.5 and 7.25 predicted by the Gaussian model.

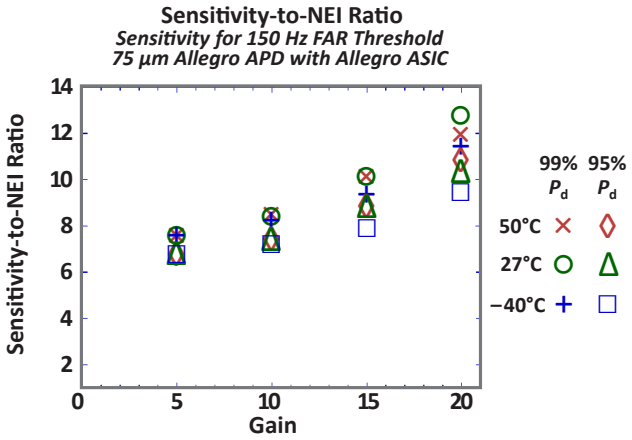

Figure 9: Ratio of sensitivity to NEI, for 150 Hz FAR, modeled from empirical Allegro 75 µm photoreceiver dark current, excess noise, and NEI data.

A similar NEI-to-sensitivity curve is presented in Figure 10, overlaid by the percent error from the Gaussian approximation. The error of the Gaussian approximation increases as the operating gain and temperature increase.

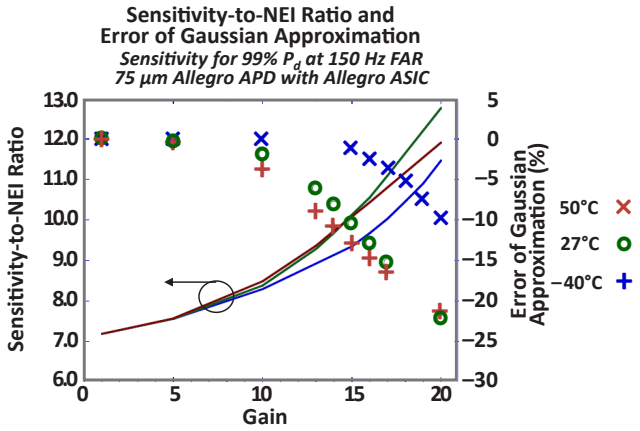

Figure 10: Ratio of sensitivity to NEI for 99% P_d, for 150 Hz FAR, with error of Gaussian approximation.

CONCLUSION

A correction to the Gaussian FAR model has been presented with estimates of the impact on calculations of sensitivity and ROC. Errors become significant as APD noise starts to dominate the total noise of the photoreceiver, which occurs at higher temperatures and avalanche gains. In such cases, numerical convolution of the APD McIntyre-distributed dark current with Gaussian-distributed TIA noise can support more accurate modeling, prior to empirical characterization of FAR versus detection threshold. The simulated results presented, which are based on measurements of Allegro APD photoreceivers, demonstrate where the limitations of the Gaussian model lie for a relevant example.

Revision History

Number	Date	Description	Responsibility
–	March 17, 2022	Initial release	A. Huntington

This document is based on the following published work:

Andrew S. Huntington, George M. Williams, and Adam O. Lee "Modeling false alarm rate and related characteristics of laser ranging and LIDAR avalanche photodiode photoreceivers," Optical Engineering 57(7), 073106 (18 July 2018). https://doi.org/10.1117/1.OE.57.7.073106

Received: 18 March 2018; Accepted: 5 June 2018; Published: 18 July 2018

MCO-0001216
P0175

955 PERIMETER ROAD • MANCHESTER, NH 03103 • USA
+1-603-626-2300 • FAX: +1-603-641-5336 • ALLEGROMICRO.COM